Structural Control of Photoinduced Energy Transfer between Adjacent and Distant Sites in Multiporphyrin Arrays

Robin K. Lammi,[†] Arounaguiry Ambroise,[‡] Thiagarajan Balasubramanian,[‡] Richard W. Wagner,[‡] David F. Bocian,*[,§] Dewey Holten,*[,†] and Jonathan S. Lindsey*[,‡]

Contribution from the Departments of Chemistry, Washington University, St. Louis, Missouri 63130-4889, North Carolina State University, Raleigh, North Carolina 27695-8204, and University of California, Riverside, California 92521-0403

Received March 23, 2000. Revised Manuscript Received May 30, 2000

Abstract: A family of diphenylethyne-linked porphyrin dimers and trimers has been prepared via a building block approach for studies of energy-transfer processes. The dimers contain Mg and Zn porphyrins (MgZnU); the trimers contain an additional free base porphyrin (MgZnFbU). In both the dimers and trimers, sites of attachment to the Mg porphyrin (at the meso- or β-position) and diphenylethyne linker (at the para- or meta-positions) were varied, producing four Mg porphyrin−Zn porphyrin arrangements with the following linker configurations: meso-p/p-meso, meso-m/p-meso, β-p/p-meso, and β-m/p-meso. All four trimers employ a meso-p/p-meso Zn porphyrin−Fb porphyrin connection. The ground- and excited-state properties of the porphyrin dimers and trimers have been examined using static and time-resolved optical techniques. The rate of energy transfer from the photoexcited Zn porphyrin to the Mg porphyrin decreases according to the following trend: meso-p/p-meso $(9\ \text{ps})^{-1}$ > β-p/p-meso $(14\ \text{ps})^{-1}$ > meso-m/p-meso $(19\ \text{ps})^{-1}$ > β-m/p-meso $(27\ \text{ps})^{-1}$. In each compound, energy transfer between adjacent porphyrins occurs through a linker-mediated through-bond process. The rate of energy transfer between Zn and Fb porphyrins is constant in each trimer ($(24\ \text{ps})^{-1}$). Energy transfer from the photoexcited Zn porphyrin branches to the adjacent Fb and Mg porphyrins, with nearly one-half to three-fourths proceeding to the Mg porphyrin (depending on the linker). Energy transfer from the excited Mg porphyrin to the nonadjacent Fb porphyrin occurs more slowly, with a rate that follows the same trend in linker architecture and porphyrin connection site: meso-p/p-meso $(173\ \text{ps})^{-1}$ > β-p/p-meso $(225\ \text{ps})^{-1}$ > meso-m/p-meso $(320\ \text{ps})^{-1}$ > β-m/p-meso $(385\ \text{ps})^{-1}$. The rate of transfer between nonadjacent Mg and Fb porphyrins does not change significantly with temperature, indicating a superexchange mechanism utilizing orbitals/states on the intervening Zn porphyrin. Energy transfer between nonadjacent sites may prove useful in directing energy flow in multiporphyrin arrays and related molecular photonic devices.

I. Introduction

As part of a program in molecular photonics, we have been developing multiporphyrin arrays that serve as molecular photonic wires,[1] optoelectronic gates,[2] and light-harvesting funnels.[3−8] To better understand and selectively modify rates and efficiencies of electronic communication in these devices, we have been investigating the photophysical properties of their constituent elements.[8−18] Previous studies on porphyrin dimers have examined several architectural alterations (identity of central metal ion, electron-donating/withdrawing character of nonlinking substituents, linker type, steric hindrance on diarylethyne linkers, linker−porphyrin attachment sites) which have

[†] Washington University.
[‡] North Carolina State University.
[§] University of California.

(1) Wagner, R. W.; Lindsey, J. S. *J. Am. Chem. Soc.* **1994**, *116*, 9759−9760.
(2) Wagner, R. W.; Lindsey, J. S.; Seth, J.; Palaniappan, V.; Bocian, D. F. *J. Am. Chem. Soc.* **1996**, *118*, 3996−3997.
(3) Li, J.; Ambroise, A.; Yang, S. I.; Diers, J. R.; Seth, J.; Wack, C. R.; Bocian, D. F.; Holten, D.; Lindsey, J. S. *J. Am. Chem. Soc.* **1999**, *121*, 8927−8940.
(4) Li, J.; Diers, J. R.; Seth, J.; Yang, S. I.; Bocian, D. F.; Holten, D.; Lindsey, J. S. *J. Org. Chem.* **1999**, *64*, 9090−9100.
(5) Li, J.; Lindsey, J. S. *J. Org. Chem.* **1999**, *64*, 9101−9108.
(6) Kuciauskas, D.; Liddell, P. A.; Johnson, T. E.; Weghorn, S. J.; Lindsey, J. S.; Moore, A. L.; Moore, T. A.; Gust, D. *J. Am. Chem. Soc.* **1999**, *121*, 8604−8614.
(7) Li, F.; Yang, S. I.; Ciringh, Y.; Seth, J.; Martin, C. H., III; Singh, D. L.; Kim, D.; Birge, R. R.; Bocian, D. F.; Holten, D.; Lindsey, J. S. *J. Am. Chem. Soc.* **1998**, *120*, 10001−10017.
(8) Li, F.; Gentemann, S.; Kalsbeck, W. A.; Seth, J.; Lindsey, J. S.; Holten, D.; Bocian, D. F. *J. Mater. Chem.* **1997**, *7*, 1245−1262.
(9) Strachan, J. P.; Gentemann, S.; Seth, J.; Kalsbeck, W. A.; Lindsey, J. S.; Holten, D.; Bocian, D. F. *J. Am. Chem. Soc.* **1997**, *119*, 11191−11201.
(10) Strachan, J.-P.; Gentemann, S.; Seth, J.; Kalsbeck, W. A.; Lindsey, J. S.; Holten, D.; Bocian, D. F. *Inorg. Chem.* **1998**, *37*, 1191−1201.
(11) Yang, S. I.; Lammi, R. K.; Seth, J.; Riggs, J. A.; Arai, T.; Kim, D.; Bocian, D. F.; Holten, D.; Lindsey, J. S. *J. Phys. Chem. B* **1998**, *102*, 9426−9436.
(12) Yang, S. I.; Seth, J.; Balasubramanian, T.; Kim, D.; Lindsey, J. S.; Holten, D.; Bocian, D. F. *J. Am. Chem. Soc.* **1999**, *121*, 4008−4018.
(13) Hascoat, P.; Yang, S. I.; Lammi, R. K.; Alley, J.; Bocian, D. F.; Lindsey, J. S.; Holten, D. *Inorg. Chem.* **1999**, *38*, 4849−4853.
(14) Yang, S. I.; Seth, J.; Strachan, J.-P.; Gentemann, S.; Kim, D. H.; Holten, D.; Lindsey, J. S.; Bocian, D. F. *J. Porphyrins Phthalocyanines* **1999**, *3*, 117−147.
(15) Hsiao, J.-S.; Krueger, B. P.; Wagner, R. W.; Johnson, T. E.; Delaney, J. K.; Mauzerall, D. C.; Fleming, G. R.; Lindsey, J. S.; Bocian, D. F.; Donohoe, R. J. *J. Am. Chem. Soc.* **1996**, *118*, 11181−11193.
(16) Wagner, R. W.; Johnson, T. E.; Lindsey, J. S. *J. Am. Chem. Soc.* **1996**, *118*, 11166−11180.
(17) Seth, J.; Palaniappan, V.; Johnson, T. E.; Prathapan, S.; Lindsey, J. S.; Bocian, D. F. *J. Am. Chem. Soc.* **1994**, *116*, 10578−10592.
(18) Seth, J.; Palaniappan, V.; Wagner, R. W.; Johnson, T. E.; Lindsey, J. S.; Bocian, D. F. *J. Am. Chem. Soc.* **1996**, *118*, 11194−11207.

10.1021/ja001031x CCC: $19.00
Published on Web 07/21/2000

Chart 1. Structures of Linear and T-Shaped Optoelectronic Gates

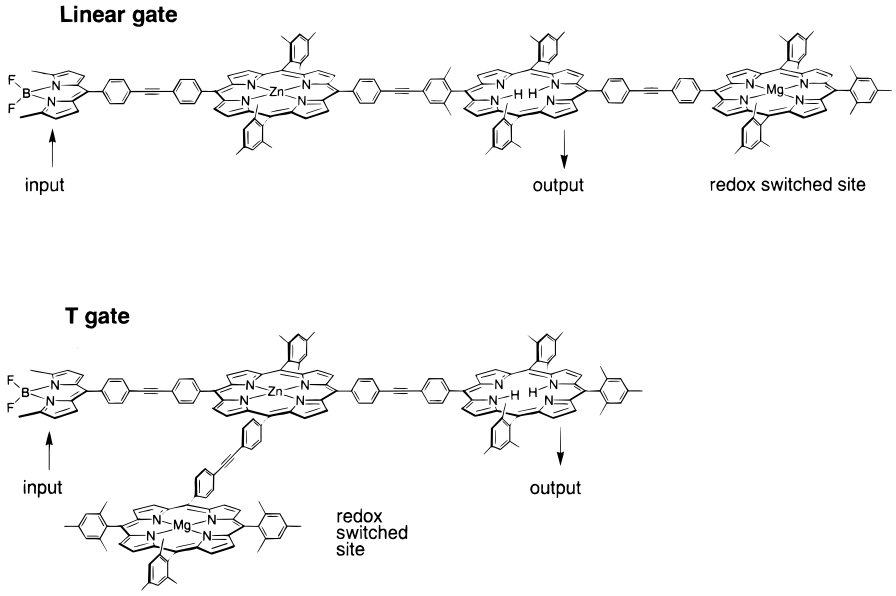

been shown to influence interporphyrin electronic communication.[8−13]

An examination of two different architectures of optoelectronic gates has prompted further studies of electronic communication in multiporphyrin arrays. The two types of prototypical molecular optoelectronic gates are shown in Chart 1.[2] Each is composed of a molecular photonic wire that serves to transmit excited-state energy and a redox-switched site where the energy flow can be turned on and off, either chemically or electrochemically. The wire consists of a boron−dipyrrin input element, a Zn porphyrin transmission element, and a free base (Fb) porphyrin output element; a Mg porphyrin acts as the redox-switched unit. In the linear gate, the Mg porphyrin is appended to the Fb porphyrin, while in the T gate, the Mg porphyrin is attached to the Zn porphyrin. In both arrays, photoexcitation of the boron−dipyrrin chromophore results in fluorescence emission from the Fb porphyrin output element; upon oxidation of the Mg porphyrin, this fluorescence diminishes by more than a factor of 30. The similar behavior of the linear and T gates raised questions concerning the extent of interaction between the Mg and Fb porphyrins via the intervening Zn porphyrin. Additional evidence for such an interaction stemmed from simple fluorescence experiments: excitation of the Mg porphyrin in the T gate resulted in a high yield of energy transfer to the Fb porphyrin, even though the intervening Zn porphyrin lies at higher energy.

To our knowledge, an investigation of energy transfer between nonadjacent sites in trimeric or larger arrays has not been reported. While the question of whether energy transfer occurs between nonadjacent sites in covalently linked architectures is of great interest, characterizing such nonpairwise interactions requires, at the minimum, an array containing three components having different excited-state energies and distinct spectral features. The vast majority of studies aimed at understanding energy transfer in multiporphyrin architectures have focused on dimers and larger arrays containing no more than two different types of porphyrins.

In this paper, we extend our investigation of energy transfer in multiporphyrin arrays via an examination of a family of diphenylethyne-linked porphyrin trimers comprised of one Mg, one Zn, and one Fb porphyrin. These MgZnFbU trimers employ different connectivities of the linker joining the Mg and Zn porphyrins. Attachment to the Mg porphyrin is made at the meso- or β-position, while attachment to the phenyl rings of the linker between the Mg and Zn porphyrins is made at the para- or meta-positions. The four resulting Mg−linker−Zn arrangements are as follows: meso-p/p-meso, β-p/p-meso, meso-m/p-meso, and β-m/p-meso; each trimer has a linker with meso-p/p-meso connectivity between the Zn and Fb porphyrins (Chart 2). As benchmarks for the trimers, we have also prepared and studied a corresponding set of Mg−Zn porphyrin dimers (Chart 3). Our goals in the investigation of these compounds were to (1) compare the rates and efficiencies of electronic communication obtained for the four different architectures and (2) investigate the rates and mechanism(s) of energy transfer between the nonadjacent Mg and Fb porphyrins in the trimers. Collectively, the present studies both improve our understanding of the operation of the optoelectronic gates and reveal strategies for achieving increased flexibility and control in the design of future molecular photonic devices.

II. Results

Synthesis. (a) Strategy. We have developed a modular approach for the synthesis of multiporphyrin arrays joined by diphenylethyne linkers.[16,19] This approach relies on the use of ethyne- or iodo-substituted porphyrin building blocks. The porphyrins are employed in defined metalation states (Mg, Zn, Fb) and are joined under conditions that do not alter the metalation state. The coupling reaction proceeds under mild conditions that are slightly basic. For the synthesis of the dimers, the iodo or ethyne groups could be positioned equally well on the Mg porphyrin or the Zn porphyrin; however, Mg porphyrins are more labile than Zn porphyrins, and this difference in chemical stability has ramifications in the synthesis plan for the trimers. The synthesis of the MgZnFb trimers, which requires a stepwise procedure employing three porphyrin building blocks, in principle could proceed from the Fb porphyrin end or the Mg porphyrin end. To minimize handling of the Mg porphyrin, the synthesis beginning at the Fb porphyrin is strongly preferred. Thus, a Fb mono-ethynyl porphyrin is coupled with a Zn

(19) Lindsey, J. S. In *Modular Chemistry*; Michl, J., Ed.; NATO ASI Series C: Mathematical and Physical Sciences, Vol. 499; Kluwer Academic Publishers: Dordrecht, 1997; pp 517−528.

Chart 2. Structures of MgZnFbU Trimers Employing Various Attachment Architectures (Nomeclature for Linker Structure and Site of Connection Is Listed below Each Trimer)

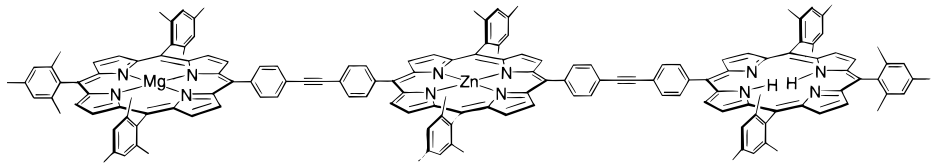

MgZnFbU meso-p/p-meso

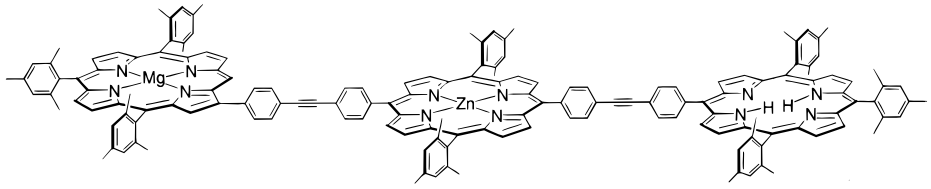

MgZnFbU β-p/p-meso

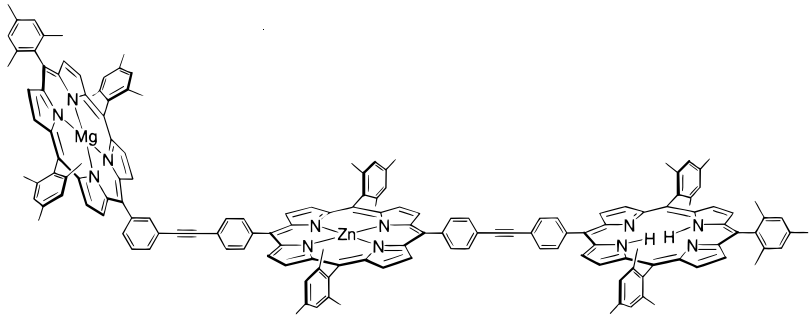

MgZnFbU meso-m/p-meso

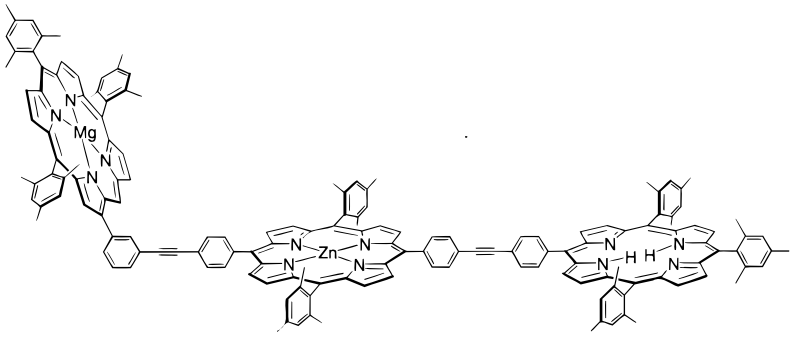

MgZnFbU β-m/p-meso

porphyrin bearing an iodo group and a trimethylsilyl-protected ethyne group. Subsequent deprotection affords the mono-ethynyl ZnFb dimer, which is then coupled with a mono-iodo Mg porphyrin. The preparation of the four MgZnFb trimers thus makes use of one mono-ethynyl ZnFb dimer and four different mono-iodo Mg porphyrins (Chart 4). The same Mg porphyrins are employed in the synthesis of the four dimers. We have previously described the syntheses of MgZnFbU meso-p/p-meso and MgZnU-meso-p/p-meso via this strategy.[20] The synthesis of the other trimers and dimers requires access to the requisite mono-iodo porphyrins.

(b) Synthesis of Monoiodo Mg Porphyrins. The Fb porphyrin bearing one meso-(*m*-iodophenyl) substituent has been synthesized previously by mixed aldehyde condensation of *m*-iodobenzaldehyde, mesitaldehyde, and pyrrole.[3] The synthesis of the β-substituted porphyrins required access to the corresponding β-substituted dipyrromethanes. We have previously prepared the Fb porphyrin bearing one β-(*p*-iodophenyl) substituent,[21] and the same strategy was employed to prepare the Fb porphyrin bearing one β-(*m*-iodophenyl) substituent. Thus, reaction of *m*-iodobenzaldehyde and monoethyl malonate under Knoevenagal conditions afforded ethyl 3-iodocinnamate (**1**) in 85% yield, which upon treatment with tosylmethylisocyanide under van Leusen's methodology[22] afforded 3-ethyoxycarbonyl-4-(3-iodophenyl)pyrrole (**2**) in 70% yield (Scheme 1). Acid-catalyzed coupling of **2** and *N*-Boc-2-hydroxymethylpyrrole in dioxane yielded a mixture of two regioisomeric dipyrromethanes (**3a**,**b**) in 83% yield (1:1.4 ratio). Chromatographic separation

(20) Wagner, R. W.; Ciringh, Y.; Clausen, C.; Lindsey, J. S. *Chem. Mater.* **1999**, *11*, 2974−2983.

(21) Balasubramanian, T.; Lindsey, J. S. *Tetrahedron* **1999**, *55*, 6771−6784.

(22) van Leusen, A. M.; Siderius, H.; Hoogenboom, B. E.; van Leusen, D. *Tetrahedron Lett.* **1972**, 5337−5340.

Chart 3. Structures of MgZnU Dimers Employing Various Attachment Architectures (Nomenclature for Linker Structure and Site of Connection Is Listed below Each Dimer)

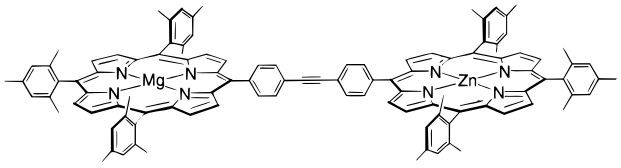

MgZnU meso-p/p-meso

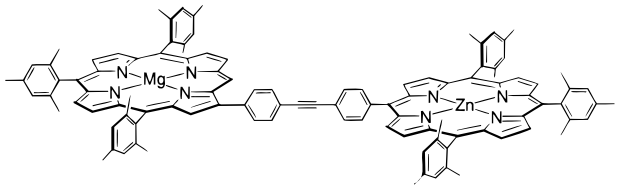

MgZnU β-p/p-meso

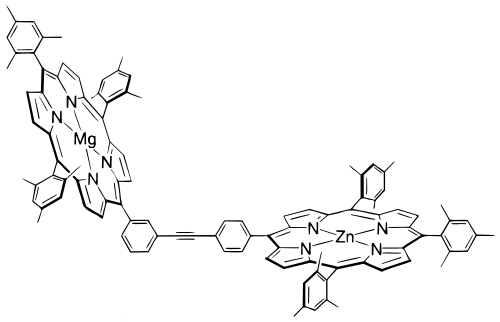

MgZnU meso-m/p-meso

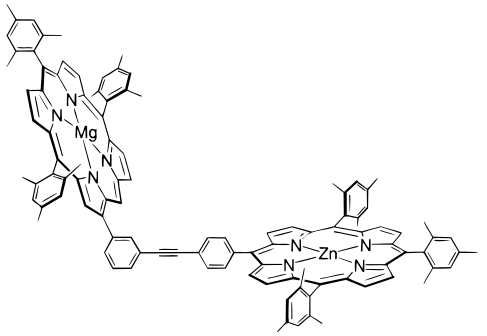

MgZnU β-m/p-meso

afforded the required dipyrromethane (**3b**). Treatment of **3b** at 200 °C in ethylene glycol containing NaOH for 1 h caused saponification, decarboxylation, and deprotection, affording the desired β-substituted dipyrromethane (**4**) in 65% yield. The reaction of **4**, 5-mesityldipyrromethane, and mesitaldehyde under porphyrin-forming conditions (condensation via $BF_3 \cdot OEt_2$ in $CHCl_3$ for 1 h followed by oxidation with DDQ)[23] afforded a mixture of three porphyrins as determined by TLC analysis and laser desorption mass spectrometry (LD-MS). (Note that the two putative porphyrin isomers that can form by condensation of mesitaldehyde and **4** were not resolved by TLC and are undetectable by LD-MS.) Separation of the porphyrins by chromatography was difficult. Conversion of the porphyrins to the respective zinc chelates enabled straightforward separation by chromatography on alumina, affording the ZnI β-m product in 12% yield. Treatment with TFA in CH_2Cl_2 afforded the desired Fb porphyrin FbI β-m in 78% yield (Scheme 2).

(23) Lindsey, J. S.; Wagner, R. W. *J. Org. Chem.* **1989**, *54*, 828−836.

Chart 4. Mg Porphyrin Building Blocks

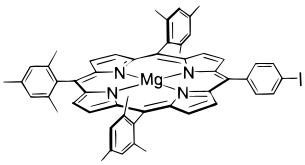

MgI meso-p

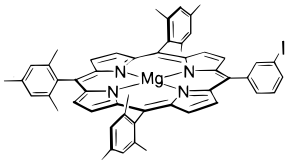

MgI meso-m

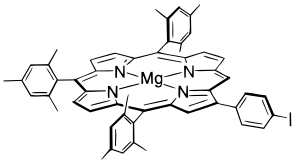

MgI β-p

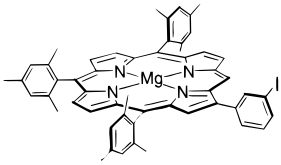

MgI β-m

The Fb porphyrins were converted to the corresponding magnesium chelates using the heterogeneous room-temperature magnesium insertion method.[24] Thus, treatment of a Fb porphyrin with MgI_2 and *N*,*N*-diisopropylethylamine in CH_2Cl_2 for 30 min, followed by chromatographic workup on alumina (grade V) with acid-free $CHCl_3$, gave the corresponding magnesium porphyrin in yields of around 80%. Note that it is essential to employ alumina rather than silica in chromatographing magnesium porphyrins, as silica affords facile demetalation of magnesium porphyrins.[4,25]

(c) Synthesis of the MgZn Dimers. Each MgZn dimer was prepared by Pd-mediated coupling of the mono-ethynyl Zn porphyrin with the desired mono-iodo Mg porphyrin (Scheme 3). We have recently developed refined conditions for the Pd-coupling reaction that afford minimal byproducts.[20] Application of this method (2.5 mM porphyrin substrates, $Pd_2(dba)_3$, P(*o*-tol)$_3$ in toluene/triethylamine 5:1, 35 °C, no copper cocatalysts) gave good coupling yields. The progress of the reaction was monitored by analytical size exclusion chromatography (SEC). The porphyrin dimers were purified by chromatographic workup involving (1) removal of Pd species by filtration over alumina, (2) separation by size on a preparative SEC column using toluene, and (3) final cleanup by chromatography on alumina. In this manner, the dimers MgZnU β-p/p-meso, MgZnU meso-m/p-meso, and MgZnU β-m/p-meso were prepared in yields of approximately 60%. The purity of each dimer was checked by analytical SEC, ^{1}H NMR spectroscopy, LD-MS, and FAB-MS.

(d) Synthesis of the MgZnFb Trimers. The synthesis of the trimers relied on the same Pd-mediated coupling reaction used with the dimers. Thus, the reaction of the mono-ethynyl ZnFb dimer[20] and the desired mono-iodo Mg porphyrin afforded the MgZnFb trimer (Scheme 4). After completion of the reaction, analytical SEC showed a major peak corresponding to the trimer, two minor peaks corresponding to the monomer

(24) Lindsey, J. S.; Woodford, J. N. *Inorg. Chem.* **1995**, *34*, 1063−1069.

(25) O'Shea, D. F.; Miller, M. A.; Matsueda, H.; Lindsey, J. S. *Inorg. Chem.* **1996**, *35*, 7325−7338.

Scheme 1. Synthesis of 3-(3-Iodophenyl)dipyrromethane

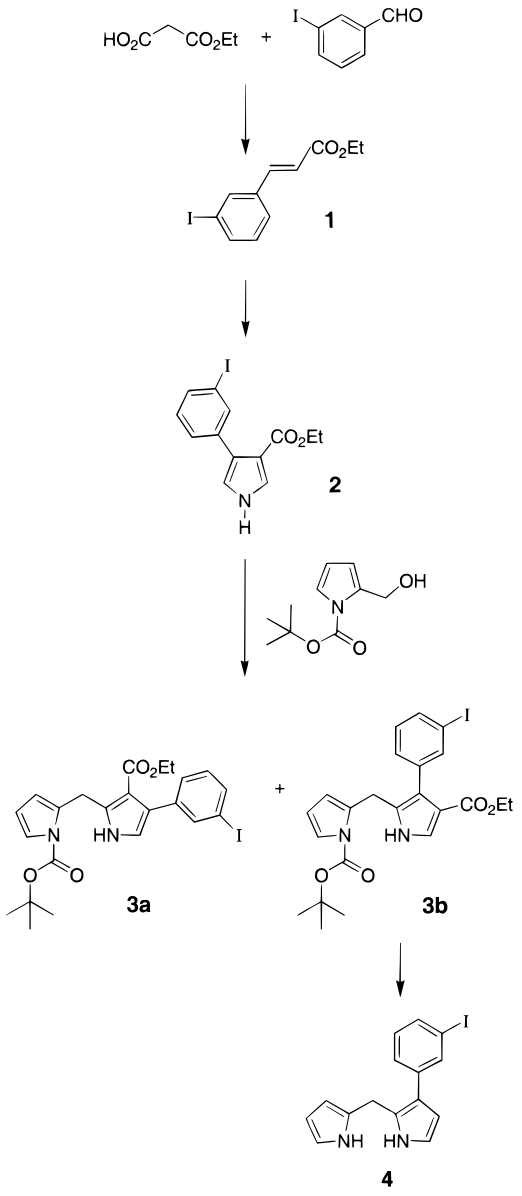

and dimer porphyrins, and a shoulder on the trimer peak due to higher molecular weight material. The reaction performed in this manner remained homogeneous. The purification scheme employed for the trimers was identical to that for the dimers except that THF rather than toluene was used in the preparative SEC process. The purity of each trimer was checked by analytical SEC, ^{1}H NMR spectroscopy, LD-MS, and FAB-MS.

Static and Time-Resolved Absorption and Emission Spectroscopy. Q-region electronic absorption and emission spectra of MgZnU meso-m/p-meso and MgZnFbU meso-m/p-meso, a representative dimer and trimer, are shown in Figure 1. The features correspond to transitions between the ground states and the lowest excited singlet states of the constituent Mg, Zn, and Fb porphyrins. The dimer absorption spectra (Figure 1a) contain the Mg porphyrin Q(1,0) band at 562 nm, the Mg porphyrin Q(0,0) band at 602 nm, and Zn porphyrin Q(1,0) and Q(0,0) peaks at 551 and 589 nm, respectively. In the trimers (Figure 1b), these Mg and Zn porphyrin features are accompanied by four Fb porphyrin bands: $Q_y(1,0)$ at 514 nm, $Q_y(0,0)$ at 551 nm, $Q_x(1,0)$ at 591 nm, and $Q_x(0,0)$ at 649 nm.

Fluorescence spectra of the dimers (Figure 1a, dashed line) exhibit a Mg porphyrin Q(0,0) emission at 605 nm and a Mg

Scheme 2. Synthesis of the β/m-Substituted Free Base Porphyrin Building Block

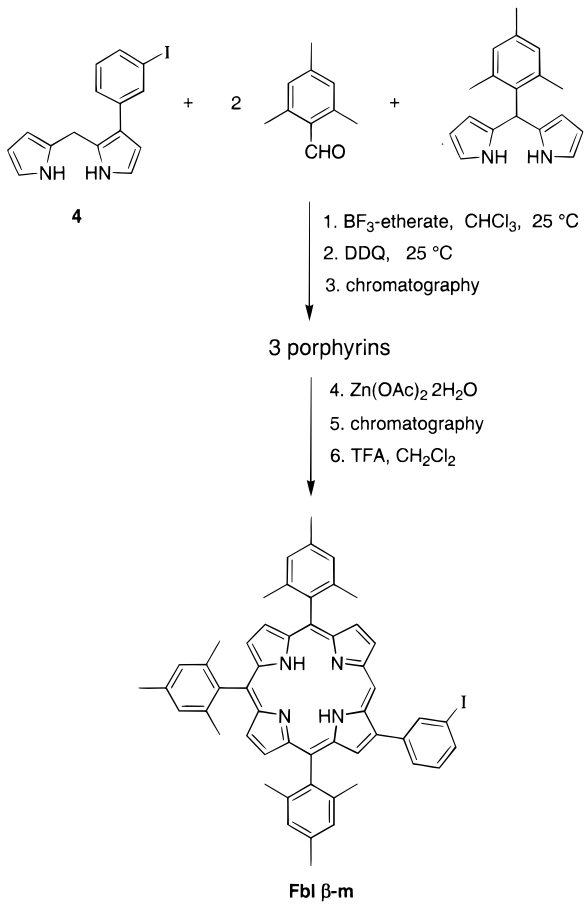

Scheme 3. Synthesis of MgZnU Dimers with Different Linker Structures and Sites of Connection

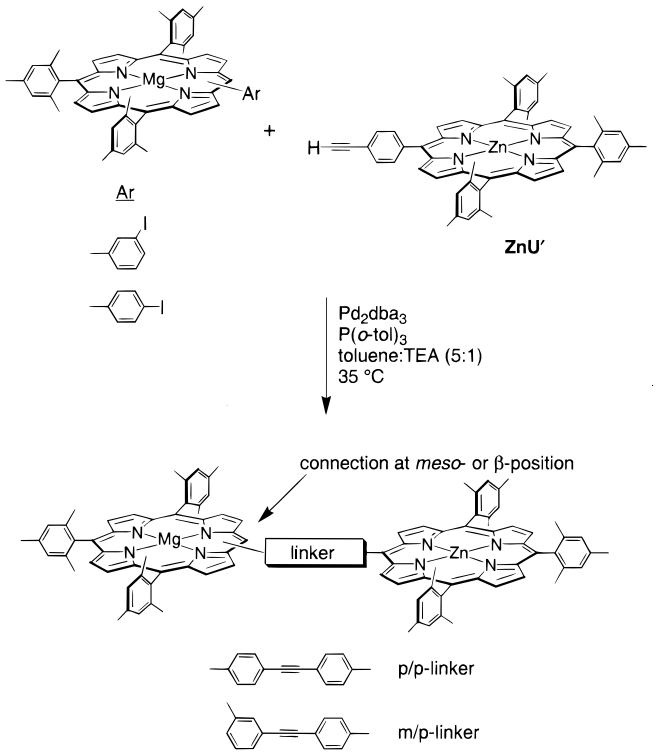

porphyrin Q(0,1) band at 660 nm. In addition to these features, the trimer spectra also contain the Fb porphyrin Q(0,0) emission

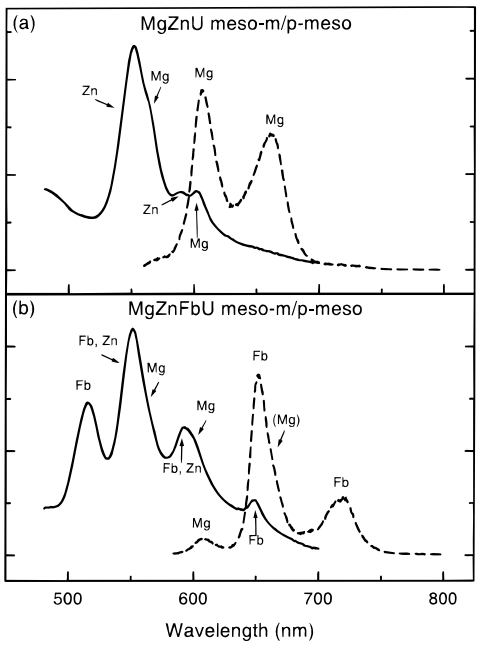

Figure 1. Q-region absorption (solid line) and emission spectra (dashed line) in toluene at room temperature: (a) MgZnU meso-m/p-meso, for emission, $\lambda_{ex} = 542$ nm; (b) MgZnFbU meso-m/p-meso, for emission, $\lambda_{ex} = 569$ nm.

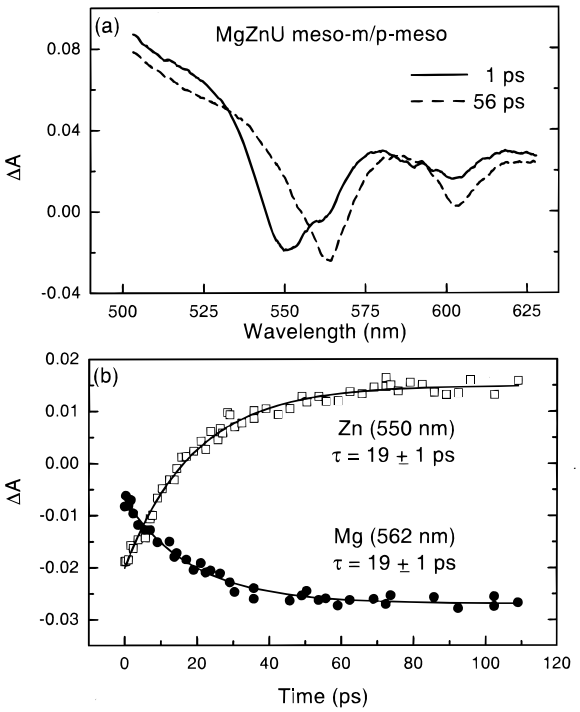

Figure 2. (a) Representative time-resolved absorption difference spectra for MgZnU meso-m/p-meso in toluene at room temperature elicited by excitation with a 130 fs flash at 542 nm. (b) Representative kinetic data (550 and 562 nm) and fits. For clarity, data before zero time and during the instrument rise are not shown.

at 651 nm and the Fb porphyrin Q(0,1) peak at 720 nm. Note that fluorescence from the MgZnU dimers occurs nearly exclusively from the Mg porphyrin, even when the Zn porphyrin is preferentially excited. This indicates that energy transfer from the photoexcited Zn porphyrin to the ground-state Mg porphyrin (denoted Zn* → Mg) is effectively quantitative. Similarly high efficiencies were noted previously for the meso-p/p-meso dimers MgZnU, ZnFbU, and MgFbU.[8,13,15] In the case of the MgZnFbU trimers (Figure 1b, dashed line), emission is detected predominantly from the free base porphyrin. No Zn* emission occurs; however, a small amount of Mg porphyrin emission is evident when the Mg component is excited. This suggests that photoinduced energy transfer from Mg* to Fb is slightly less than quantitative.

The rates and efficiencies of photoinduced energy transfer for the series of MgZnU dimers and MgZnFbU trimers were quantitated using time-resolved absorption measurements. Procedures and analyses were similar to those described previously for other multiporphyrin arrays.[8−15] In the dimers, the Zn porphyrin was photoexcited in order to observe Zn* → Mg energy transfer. Results from a representative experiment on MgZnU meso-m/p-meso are shown in Figure 2. The absorption difference spectrum at 1 ps after excitation with a 130 fs flash at 542 nm shows predominantly bleaching of the Zn porphyrin

Scheme 4. Synthesis of MgZnFbU Trimers with Different Linker Structures and Sites of Connection

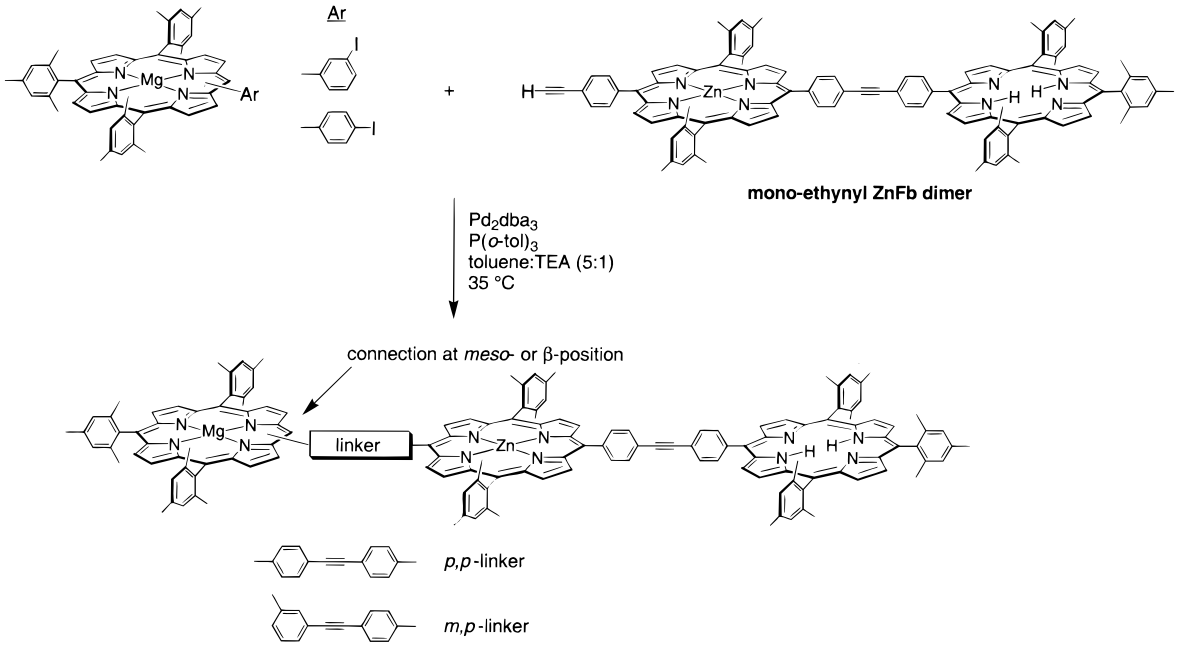

Table 1. Photophysical Data for Dimers and Monomer Reference Compounds[a]

	τ (ps)			
dimers	Zn* [b]	Mg* [b]	k_{trans}^{-1} (ps)[c]	Φ_{trans}[d]
MgZnU				
meso-p/p-meso	9 ± 1[f]		9[f]	>0.99[f]
β-p/p-meso	14 ± 1		14	>0.99
meso-m/p-meso	19 ± 1		19	>0.99
β-m/p-meso	27 ± 2		27	0.99
ZnFbU[g]				
meso-p/p-meso	24 ± 2[f]		24[f]	0.99[f]
meso-m/p-meso	39 ± 4[h]		40[h]	0.98[h]
β-p/p-β	55 ± 5[i]		56[i]	0.98[i]
MgFbU[g]				
meso-p/p-meso		31 ± 3[f]	31[f]	>0.99[f]

	τ (ns)		
monomers[j]	Zn* [e]	Mg* [e]	Fb* [e]
MgU′		9.7 ± 0.4[f]	
ZnU′	2.4 ± 0.2[k]		
ZnU′-β[l]	2.4 ± 0.2[i]		
FbU′			13.3 ± 0.5[k]

[a] Data in toluene at room temperature. [b] Zn* and Mg* (donor) lifetimes in dimers measured by transient absorption spectroscopy. [c] Inverse of the energy-transfer rate calculated from eq 3 and lifetimes in table. [d] Energy-transfer efficiency calculated from eq 4. [e] Zn*, Mg*, and Fb* lifetimes in monomers measured by time-resolved emission spectroscopy. [f] From ref 13. [g] Nomenclature for ZnFbU and MgFbU dimers is the same as for MgZnU dimers; see Chart 2. [h] From ref 3. [i] From ref 12. [j] See structure of U′ monomers in Chart 5. [k] From ref 14. [l] Zn(II) 5,10,15-trimesityl-2-(4-ethynylphenyl)porphyrin.

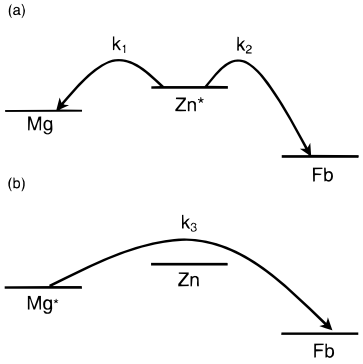

Figure 3. Diagram of energy-transfer processes in MgZnFbU trimers. (a) Excitation of the Zn porphyrin results in branching of the flow of energy (Zn* → Mg and Zn* → Fb). (b) Excitation of the Mg porphyrin results in Mg* → Fb energy transfer.

Q(1,0) ground-state band at 551 nm; there is also a small bleaching of the Mg porphyrin Q(1,0) ground-state band at 562 nm due to Mg-porphyrin excitation in a small fraction of dimers. The Zn porphyrin bleaching decays between 1 and 56 ps, while the Mg porphyrin bleaching develops. Data were fit to a single-exponential function, giving a time constant of 19 ± 1 ps for the Zn* lifetime in the dimer. This result is listed in Table 1 along with those of the other MgZnU dimers; also included are lifetime data for related dimers and monomer building blocks.

Several energy-transfer processes occur in each trimer: (1) Zn* → Mg, (2) Zn* → Fb, both of which occur between adjacent porphyrins, and (3) Mg* → Fb, which occurs between nonadjacent porphyrin units (Figure 3). Since neither the Zn nor the Mg porphyrin can be exclusively excited (due to overlapping Q(1,0) and Q(0,0) absorption bands), dual-exponential decays were expected. To clearly determine time constants for the decays of the Zn* and Mg* excited states, two experiments were performed on each trimer. In one, the Zn porphyrin was preferentially excited (at 542 nm, forming MgZn*Fb in most of the molecules and Mg*ZnFb in a small number); in the other experiment, primarily the Mg porphyrin was excited (at 569 nm). Both experiments on a given trimer were expected to yield similar results. More confidence was placed in the 542 nm excitation for determination of the Zn* lifetime and in the 569 nm excitation for the Mg* lifetime, due to the larger amplitude of the respective kinetic component in the dual-exponential fits. Absorption difference spectra and kinetics traces for representative experiments on MgZnFbU meso-m/p-meso are shown in Figure 4. Spectra in panel a (542 nm excitation) clearly show the decay of the Zn porphyrin Q(1,0) ground-state bleaching at 541 nm and the growth of the Fb porphyrin Q_y(1,0) ground-state bleaching at 514 nm over time. Less clear are the growth of the Mg porphyrin Q(1,0) ground-state bleaching at 562 nm that occurs between 1 and 96 ps and its subsequent decay between 96 ps and 2.3 ns after excitation. These processes are more evident in the spectra in panel c (569 nm excitation), in which the Mg porphyrin was preferentially excited. The Mg porphyrin Q(1,0) ground-state bleaching decays, disappearing between 96 ps and 2.3 ns after excitation, while the Fb porphyrin Q_y(1,0) and Q_y(0,0) ground-state bleachings grow in with time. Kinetic analysis of data in several spectral regions from each experiment gave similar results, as anticipated. Both sets of kinetic data were fit to two exponentials (plus a constant): the short component of 9 ± 1 ps corresponds to the Zn* lifetime and the longer component of 310 ± 30 ps corresponds to the Mg* lifetime. (These are average values that take into account the results of experiments with 542 and 569 nm excitation.) Zn* and Mg* lifetimes for the other trimers were determined in the same manner and are listed in Table 2. Note that if no energy transfer occurred from Mg*, the Mg* lifetime in each of the trimers would be expected to be equal to that of a monomeric Mg porphyrin (9.7 ns).

Table 2. Excited-State Lifetimes in MgZnFbU Trimers[a]

	τ (ps)		
MgZnFbU trimer	Zn* [b]	Zn* (calcd)[c]	Mg* [b]
meso-p/p-meso[d]	7 ± 1	6.5	170 ± 30
β-p/p-meso	11 ± 3	8.8	220 ± 30
meso-m/p-meso	9 ± 1	10.3	310 ± 30
β-m/p-meso	13 ± 4	12.7	370 ± 50

[a] Data in toluene at room temperature. [b] Zn* and Mg* lifetimes measured by transient absorption spectroscopy. [c] Zn* lifetime calculated from eq 5 and values in Table 1. [d] This compound was more difficult to work with than the other trimers, exhibiting lower solubility due to aggregation.

Low-temperature experiments were carried out on MgZnFbU meso-m/p-meso in toluene, at 200 K (just above the freezing point), and in 2-methyltetrahydrofuran (2-MeTHF), at 79 K. The objective of these experiments was to examine energy transfer from the photoexcited Mg porphyrin to the nonadjacent Fb porphyrin, so as to elucidate the mechanism of this process: either a two-step hopping mechanism in which Zn* is formed, or a one-step superexchange mechanism using orbitals/states on the Zn porphyrin. As such, we chose to excite the Mg porphyrin preferentially (at 569 nm). Kinetic analysis of data in several spectral regions revealed double-exponential decays; again, the short component corresponds to the Zn* lifetime and the long one to the Mg* lifetime. Values for the Mg* lifetimes determined are listed in Table 3, along with room-temperature results in the same solvents. It is apparent from these results that the Mg* lifetime is not very temperature-dependent.

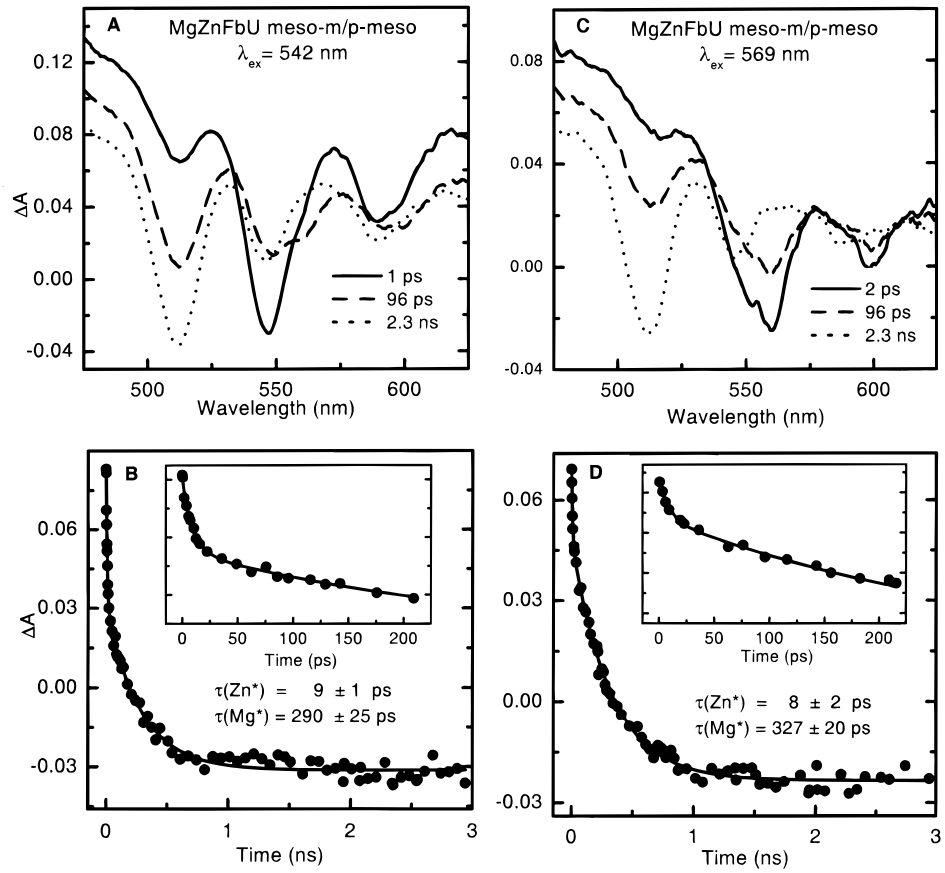

Figure 4. Representative time-resolved absorption spectra, kinetic data at 513 nm, and fits for MgZnFbU meso-m/p-meso in toluene. Panels a and b show the results of excitation at 542 nm; spectra and kinetics shown in panels c and d were obtained by exciting at 569 nm. Average Zn* and Mg* lifetimes were determined from analysis of several spectral regions in each experiment and are listed in Table 2.

Table 3. Temperature Dependence of Mg* Lifetimes in MgZnFbU meso-m/p-meso

solvent	temperature (K)	τ(Mg*)[a] (ps)
toluene	294	310 ± 30
2-MeTHF	294	250 ± 50
toluene	200	340 ± 120
2-MeTHF	79	180 ± 30

[a] Mg* lifetimes obtained from transient absorption experiments.

Excited-State Energy-Transfer Rates and Yields. The parameters for photoinduced energy transfer in the MgZnU dimers and MgZnFbU trimers were obtained using eqs 1−5,

$$1/\tau_D = k_{rad} + k_{isc} + k_{ic} \quad (1)$$

$$1/\tau_{DA} = k_{rad} + k_{isc} + k_{ic} + k_{trans} \quad (2)$$

$$k_{trans} = 1/\tau_{DA} - 1/\tau_D \quad (3)$$

$$\Phi_{trans} = k_{trans}\tau_{DA} = 1 - \tau_{DA}/\tau_D \quad (4)$$

$$1/\tau_{Zn}^{tri} = 1/\tau_D + k_{MgZn} + k_{ZnFb} \quad (5)$$

where τ_{DA} is the excited-state lifetime of the donor in the presence of the acceptor (e.g., Zn* in MgZnU meso-m/p-meso), τ_D is the excited-state lifetime of the (donor) porphyrin monomer (e.g., Zn* in ZnU′; see Chart 5), k_{trans} is the energy-transfer rate, Φ_{trans} is the energy-transfer efficiency, and τ_{Zn}^{tri} is the Zn* lifetime in the trimer. These equations assume that, other than energy transfer, there are no pathways for depopulating the excited state of the donor porphyrin in the multiporphyrin arrays

Chart 5. Structures of MU′ Monomers

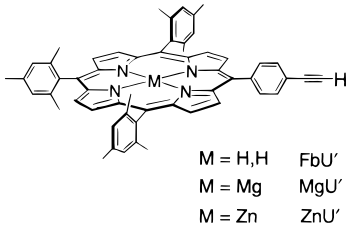

which do not also exist in the porphyrin monomers (radiative decay (rad), intersystem crossing (isc), and internal conversion (ic)). The transient absorption and static emission data support this assumption; however, we cannot exclude the possibility of a small amount of charge transfer from donor to acceptor in each array.[13]

Using eqs 1−4 and lifetime data in Table 1, photoinduced energy transfer from Zn* to Mg in MgZnU meso-m/p-meso was calculated to occur with a rate constant of (19 ps)$^{-1}$; the meso-p/p-meso and β-p/p-meso dimers have faster rates of energy transfer, while that of the β-m/p-meso compound is slower. Energy transfer is very efficient in all four dimers (≥99%). Rates and efficiencies of Zn* → Mg, Zn* → Fb, and Mg* → Fb energy transfer for these dimers and a variety of others (studied previously) are listed in Table 1.

Calculated Zn* lifetimes for the trimers that incorporate both the Zn* → Mg and Zn* → Fb pathways are listed in Table 2. These values were determined using eq 5 and the calculated energy-transfer rates for the appropriate MgZnU and ZnFbU dimers, in addition to the measured lifetime of the ZnU′ monomer (Table 1). The calculated Zn* lifetime of 10.3 ps for

Table 4. Rates and Yields of Energy Transfer in MgZnFbU Trimers[a]

	Zn* → Mg		Zn* → Fb		Mg* → Fb	
MgZnFbU trimer	k_1^{-1} (ps)[b]	ϕ_1[c]	k_2^{-1} (ps)[d]	ϕ_2[e]	k_3^{-1} (ps)[f]	Φ_3[g]
meso-p/p-meso	9	0.73	24	0.27	173	0.98
β-p/p-meso	14	0.63	24	0.37	225	0.98
meso-m/p-meso	19	0.56	24	0.44	320	0.97
β-m/p-meso	27	0.47	24	0.53	385	0.96

[a] All values calculated from results in toluene at room temperature. Processes 1, 2, and 3 are identified in Figure 3. [b] Inverse of energy-transfer rate in MgZnU dimer employing the same linker (Table 1). [c] Branching ratio for flow of energy from Zn* to Mg; for MgZnFbU meso-p/p-meso, $\phi_1 = (1/9)/(1/9 + 1/24) = 0.73$. [d] Inverse of energy-transfer rate in ZnFbU meso-p/p-meso. [e] Branching ratio for flow of energy from Zn* to Fb, calculated in the same manner as in footnote *c*. [f] Inverse of energy-transfer rate calculated from eq 3, using Mg* lifetimes in trimer and MgU′ monomer (Tables 1 and 2). [g] Energy-transfer efficiency, calculated from eq 4.

MgZnFbU meso-m/p-meso is in good agreement with the measured value of 9 ± 1 ps. Values calculated for the other three trimers also agree well with experimental results (Table 2).

In the MgZnFbU trimers, branching ratios are readily calculated (eqs 6−8) for energy transfer from Zn* to the Mg (ϕ_1) and Fb (ϕ_2) porphyrins (see Figure 3).

$$k_1/(k_1 + k_2) = \phi_1 \tag{6}$$

$$k_2/(k_1 + k_2) = \phi_2 \tag{7}$$

$$\phi_1 + \phi_2 = 1 \tag{8}$$

In each trimer, the Zn* → Fb energy-transfer rate is constant ((24 ps)$^{-1}$), due to use of the same meso-p/p-meso linker architecture, while the Zn* → Mg energy-transfer rate is altered with the different arrangements. This latter rate ranges from (9 ps)$^{-1}$ to (27 ps)$^{-1}$, giving a branching ratio that ranges from 0.73:0.27 (MgZnFbU meso-p/p-meso) to 0.47:0.53 (MgZnFbU β-m/p-meso) for flow of energy to the Mg vs Fb porphyrin (Table 4).

The rates and efficiencies of Zn porphyrin-mediated Mg* → Fb energy transfer were calculated using the measured Mg* lifetimes in the trimers and that of the MgU′ reference monomer (Tables 1 and 2). For example, MgZnFbU meso-m/p-meso has a Zn porphyrin-mediated Mg* → Fb energy-transfer rate of (320 ps)$^{-1}$, with an efficiency of 97%. Note that the slower rate of Mg* → Fb transfer compared to that of Zn* → Fb transfer ((24 ps)$^{-1}$) is mitigated by the longer lifetime of the Mg porphyrin (9.7 ns) compared to the Zn porphyrin (2.4 ns). The rates and efficiencies for Mg* → Fb transfer for the four trimers are listed in Table 4.

III. Discussion

The availability of a systematic family of arrays comprised of three porphyrins with distinct energies and spectral features has enabled study of the flow of energy between adjacent and nonadjacent sites. Static emission spectra show that excitation of the Mg or Zn porphyrins in the MgZnFbU trimers results in efficient energy transfer to the Fb porphyrin. Time-resolved data have revealed that the photoexcited Zn porphyrin transfers nearly one-half to three-fourths of its energy to the adjacent Mg porphyrin; this is followed by slower energy transfer from the excited Mg porphyrin to the nonadjacent Fb porphyrin. The observation of energy transfer between nonadjacent sites has implications for the design of molecular photonic devices comprised of multiple components in covalently linked architectures. These topics are discussed in more detail in the following sections.

Effects of Varying Porphyrin and Linker Attachment Sites. The rates and efficiencies determined for the dimers and trimers reveal an underlying trend that depends on porphyrin−linker connectivity. In the MgZnU dimers (Table 1), the rate of Zn* → Mg energy transfer decreases according to the following pattern: meso-p/p-meso (9 ps)$^{-1}$ > β-p/p-meso (14 ps)$^{-1}$ > meso-m/p-meso (19 ps)$^{-1}$ > β-m/p-meso (27 ps)$^{-1}$. The efficiency of energy transfer follows the same trend, decreasing only slightly along the series, from 0.996 for MgZnU meso-p/p-meso to 0.989 for the β-m/p-meso dimer. The family of MgZnFbU trimers exhibits the same trend in rate and efficiency of Mg* → Fb energy transfer, decreasing from (173 ps)$^{-1}$ and 0.98 for the meso-p/p-meso trimer to (385 ps)$^{-1}$ and 0.96 for the β-m/p-meso compound (Table 4). It is more difficult to clearly discern a trend in Zn* lifetime in the trimers, because the error bars in the experimental data are large enough to render the values nearly indistinguishable; however, the calculated Zn* lifetimes fit the pattern mentioned above (Table 2). Thus, the same trend in rate and efficiency of energy transfer is evident in both the dimers and trimers, and for both the Zn* → Mg and Mg* → Fb energy-transfer processes.

The findings concerning the effects of structure and connectivity on electronic communication can largely be understood by consideration of orbital interactions. In particular, attachment at the meso-position of the Mg porphyrin results in more efficient electronic communication than does connection at the β-position, and connection at the p-position of the linker is preferable to attachment at the m-position. The latter result is in agreement with previous work on ZnFbU dimers (Table 1), in which the meso-p/p-meso compound was found to have a faster rate of energy transfer than the meso-m/p-meso array ((24 ps)$^{-1}$ versus (40 ps)$^{-1}$).[3] Consideration of HOMO electron density distributions for the Mg porphyrin and the diphenylethyne linker provides a likely explanation for these findings. The majority of the electron density in the porphyrin $a_{2u}(\pi)$ HOMO is located at the meso-positions with minimal density at the β-positions.[26] Similarly, the HOMO in diphenylacetylene has electron density concentrated at the p-positions, with significantly less density at the m-positions.[27] Thus, it is reasonable that communication will be fastest and most efficient in the compounds that take advantage of both high-electron-density attachment sites (the meso-p/p-meso dimer and trimer), and slowest and least efficient in those that utilize the attachment sites with less HOMO electron density (the β-m/p-meso compounds). It is more difficult to predict the relative merit of the other two porphyrin−linker connectivities (β-p/p-meso vs meso-m/p-meso) because each of these architectures contains both favorable and unfavorable structural elements for maximizing energy-transfer rate and efficiency. Our experimental results consistently show that communication is better in β-p/p-meso compounds than in their meso-m/p-meso counterparts.

Mechanisms of Electronic Communication. Understanding the mechanism of electronic communication is essential for the rational design of molecular photonic devices. Our prior work on various families of dimers has necessarily enabled characterization of pairwise (adjacent) interactions only. The MgZnFbU trimers, which contain three porphyrins of unequal

(26) Gouterman, M. In *The Porphyrins*; Dolphin, D., Ed.; Academic: New York, 1978; Vol. III, pp 1−153.
(27) Ferrante, C.; Kensy, U.; Dick, B. *J. Phys. Chem.* **1993**, *97*, 13457−13463.

excited-state energies, enable characterization of interactions between nonadjacent porphyrin units.

Our previous studies have shown that photoinduced energy transfer between adjacent donor and acceptor porphyrins in diarylethyne-linked dimers (e.g., ZnFbU, MgFbU) occurs predominantly via an exchange-mediated through-bond (Dexter) mechanism, with a much smaller through-space (Förster) contribution.[8,9,15,28] This assessment is based on the following factors: (1) the donor excited-state lifetimes predicted by Förster calculations are on the order of 1 ns, nearly 2 orders of magnitude larger than the measured values (tens of picoseconds), and (2) energy-transfer rates depend on porphyrin−linker steric hindrance, and orbital spacing and ordering in a manner consistent with through-bond rather than through-space processes. The fact that the Zn* lifetimes in the various MgZnU dimers studied herein are also on the picosecond time scale indicates that the through-bond mechanism is likely the primary contributor in these dimers, as well. In addition, the measured Zn* lifetimes in the MgZnFbU trimers agree well with values calculated from the energy-transfer rates of constituent MgZnU and ZnFbU dimers (Table 1); therefore, it may be inferred that energy transfer between adjacent, diarylethyne-linked porphyrins in trimers and larger arrays also occurs primarily via a through-bond mechanism.

Results of static emission and transient absorption experiments (namely, emission largely due to the Fb porphyrin upon excitation of the Mg porphyrin and energy-transfer rates of $(100-400\ \text{ps})^{-1}$) have shown that there is good communication between the nonadjacent Mg and Fb porphyrins in the trimers. The finding of Mg* → Fb rates that are 2 orders of magnitude faster than the $(50\ \text{ns})^{-1}$ rate predicted for a through-space (Förster) process indicates that a through-bond mechanism involving the intervening Zn porphyrin is operable. This energy transfer between nonadjacent sites could occur by one or both of two possible mechanisms: (1) a superexchange mechanism utilizing orbitals/states on the intervening Zn porphyrin, and (2) a hopping mechanism whereby the Zn* state is actually formed from Mg*. The latter route is possible in this case because the lowest-lying Zn* excited state is only slightly higher in energy than the lowest-lying Mg* state, within 340 cm^{-1} for MgZnFbU meso-m/p-meso, a difference of 1.6 k_BT at room temperature. The rationale for the low-temperature transient absorption experiments was to examine the Mg* → Fb energy-transfer process under conditions in which thermal repopulation of Zn* was nearly impossible. (At 200 K, 340 cm^{-1} corresponds to 2.4 k_BT; at 79 K, 6.1 k_BT.) If hopping were the predominant mechanism, experiments performed at these low temperatures would show a much slower rate of Mg* → Fb energy transfer than those measured at room temperature in the same solvents. This prediction is contrary to our observations, which show that the Mg* lifetimes measured for MgZnFbU meso-m/p-meso at low temperatures were very similar to those measured at room temperature, in both toluene and 2-MeTHF (Table 3). If a very small amount of hopping does occur, it could explain why the Mg* lifetime at 79 K in 2-MeTHF may be slightly longer than that measured at 294 K (250 ± 50 versus 180 ± 30 ps). Still, it is clear that the hopping mechanism makes only a minor contribution to the observed Mg* → Fb energy-transfer process. The principal method of electronic communication between the nonadjacent, diarylethyne-linked Mg and Fb porphyrins appears to be superexchange through the orbitals/states of the intervening Zn porphyrin. To our knowledge, this is the first demonstration of non-nearest-neighbor energy transfer in multiporphyrin systems. The speed and efficiency noted here indicate that such processes may make a significant contribution to the overall energy flow in many multiporphyrin arrays.

The observation of through-bond energy transfer between nonadjacent sites in multiporphyrin arrays has significant implications for the design and characterization of molecular photonic devices. (1) Simulations aimed at accurately modeling the flow of energy in multicomponent architectures must consider the rates of pairwise and nonadjacent transfer processes. (2) The ability to transfer energy between nonadjacent sites may have advantages in some applications. For example, energy could be shunted to a pigment having a long intrinsic excited-state lifetime and subsequently released at a slower rate to a nonadjacent site. The rate of transfer can be controlled by structure, energetics, and porphyrin−linker connectivity. The MgZnFbU trimers provide a limited illustration of this case, where the monomeric Mg and Zn porphyrins have excited-state lifetimes of ∼10 and 2.4 ns, respectively. The use of other pigments with longer excited-state lifetimes can be envisioned.

IV. Conclusions

Our studies of the MgZnFbU trimers and their constituent dimers have revealed the following: (1) Attachment at the porphyrin meso-position and the *p*-phenyl position of the linker leads to the fastest, most efficient communication. (2) Rapid, efficient energy transfer occurs between nonadjacent Mg and Fb porphyrins. (3) This energy-transfer process between nonadjacent sites occurs via superexchange using orbitals/states on the Zn porphyrin. In conjunction with our previous findings regarding the through-bond energy transfer that occurs between adjacent porphyrins in diarylethyne-linked dimers (and trimers), we now have a complete picture of the processes occurring in the neutral forms of the optoelectronic gates, particularly the T gate, with its Mg−Zn−Fb porphyrin arrangement. Further understanding of gate operation will be obtained through experiments underway on dimers and trimers in which the Mg porphyrin is oxidized. Collectively, these results regarding the efficacy of different linker motifs and energy transfer between adjacent and distant porphyrins will aid in the design of larger and more complex multiporphyrin arrays for various applications in molecular photonics.

V. Experimental Methods

Synthesis. (a) General. ^{1}H NMR spectra (300 MHz), absorption spectra (HP 8451A, Cary 3), and fluorescence spectra (Spex FluoroMax) were collected routinely. Porphyrins were analyzed by laser desorption mass spectrometry (LD-MS) in the absence of a matrix.[29] Pyrrole was distilled at atmospheric pressure from CaH_2. 3-Iodobenzaldehyde was obtained from Karl Industries, Ltd.

(b) Chromatography. Adsorption column chromatography was performed using flash silica (Baker) or alumina (grade V).[8] Porphyrins were dissolved in CH_2Cl_2 for column chromatography at high concentration and then hexanes was added to achieve a nonpolar loading solvent. Preparative-scale size exclusion chromatography (SEC) was performed using Bio-Rad Bio-Beads SX-1 in a glass column (4.8 × 60 cm) packed with THF. The chromatography was performed with gravity flow (∼4 mL/min). A typical separation required ∼3 h. Following purification, the SEC column was washed with two volume equivalents of THF. Unlike adsorption columns, the SEC columns can be used repeatedly, although with continued use for porphyrin separations the columns become slightly pink-brown.

(28) Wagner, R. W.; Seth, J.; Yang, S. I.; Kim, D.; Bocian, D. F.; Holten, D.; Lindsey, J. S. *J. Org. Chem.* **1998**, *63*, 5042−5049.

(29) (a) Fenyo, D.; Chait, B. T.; Johnson, T. E.; Lindsey, J. S. *J. Porphyrins Phthalocyanines* **1997**, *1*, 93−99. (b) Srinivasan, N.; Haney, C. A.; Lindsey, J. S.; Zhang, W.; Chait, B. T. *J. Porphyrins Phthalocyanines* **1999**, *3*, 283−291.

Analytical-scale SEC was performed to assess the purity of the trimer-forming reactions and to monitor the preparative purification of the trimers. Analytical SEC columns (styrene−divinylbenzene copolymer) were purchased from Hewlett-Packard and Phenomonex. Analytical SEC was performed with a Hewlett-Packard 1090 HPLC using a 1000 Å (260 × 12 mm) column (5 μm) eluting with THF (flow rate = 0.8 mL/min). Reactions were monitored by removing aliquots from the reaction mixture and diluting with THF (Fisher, HPLC grade). Sample detection was achieved by absorption spectroscopy using a diode array detector with quantitation at 420 nm (±10 nm bandwidth), which best captures the peaks of monomeric porphyrins and the multiporphyrin arrays.

(c) Solvents. CH_2Cl_2 (Fisher, reagent grade) and $CHCl_3$ (Fisher certified ACS) were subjected to simple distillation from K_2CO_3. The commercially available $CHCl_3$ contained ethanol (0.75%) as a stabilizer. All references to $CHCl_3$ in this paper pertain to $CHCl_3$ containing 0.75% ethanol. Simple distillation does not significantly alter the ethanol content. THF (Fisher certified ACS) was distilled from sodium benzophenone ketyl as required. Toluene (Fisher certified ACS) and triethylamine (Fluka puriss) were distilled from CaH_2. THF (Fisher HPLC grade) was used for preparative SEC. Other solvents were used as received.

Ethyl 3-Iodocinnamate (1). A solution of 3-iodobenzaldehyde (5.80 g, 25.0 mmol), monoethyl malonate (5.00 g, 37.9 mmol), piperidine (0.3 mL), and pyridine (14 mL) was heated at reflux for 7 h in a 100-mL round-bottom flask. The reaction mixture was cooled to room temperature, poured into 2 N aqueous HCl (100 mL), and extracted with ether (3 × 40 mL). The ethereal portions were combined and washed successively with water (2 × 40 mL), saturated aqueous $NaHCO_3$ (2 × 40 mL), water (2 × 40 mL), and brine (50 mL). The ether portion was dried (Na_2SO_4) and evaporated to give a brownish solid. Recrystallization from absolute ethanol gave 6.50 g (85%) of a colorless solid: mp 38−39 °C; ^{1}H NMR ($CDCl_3$) δ 1.33 (t, J = 7.2 Hz, 3H), 4.26 (q, J = 7.2 Hz, 2H), 6.40 (d, J = 16.2 Hz, 1H), 7.09 (t, J = 7.2 Hz, 1H), 7.45 (d, J = 7.2 Hz, 1H), 7.48 (d, J = 16.2 Hz, 1H) 7.67 (d, J = 7.2 Hz, 1H), 7.84 (s, 1H); ^{13}C NMR ($CDCl_3$) δ 14.2, 60.5, 94.6, 119.5, 127.0, 130.3, 136.4, 136.6, 138.7, 142.6, 166.3; FAB-MS obsd 302.9885, calcd 302.9882 ($C_{11}H_{11}O_2I$). Anal. Calcd: C, 43.71; H, 3.67, Found: C, 43.92; H, 3.67.

3-Ethoxycarbonyl-4-(3-iodophenyl)pyrrole (2). To a suspension of NaH (0.60 g, 60% dispersion in mineral oil, 1.2 equiv) in 25 mL of dry ether under argon was added dropwise over 30 min a solution of **1** (3.8 g, 12.5 mmol) and tosylmethylisocyanide (TosMIC) (2.5 g, 12.8 mmol) in 60 mL of dry ether/DMSO (2:1). *Care must be exercised during addition as an exothermic reaction ensues.* The reaction mixture was stirred for an additional 30 min, carefully quenched with ice-cold water (60 mL), and extracted with ether (3 × 60 mL). The ethereal portion was dried (Na_2SO_4), filtered, and evaporated under vacuum to give a brownish solid. The crude product was purified by flash chromatography (silica, hexanes:ethyl acetate, 3:1) to give 3.0 g (70%) of a light brownish solid: mp 152−153 °C; ^{1}H NMR ($CDCl_3$) δ 1.26 (t, J = 7.2 Hz, 3H), 4.22 (q, J = 7.2 Hz, 2H), 6.76 (t, J = 2.7 Hz, 1H), 7.08 (t, J = 7.2 Hz, 1H), 7.47 (d, J = 7.2 Hz, 1H), 7.48 (t, J = 2.7 Hz, 1H) 7.60 (d, J = 8.1 Hz, 1H), 7.83 (s, 1H), 8.65 (brs, 1H); ^{13}C NMR ($CDCl_3$) δ 14.3, 59.7, 93.5, 113.8, 118.5, 124.9, 125.5, 128.7, 129.3, 135.3, 137.0, 138.0, 164.7; FAB-MS obsd 340.9934, calcd 340.9913 ($C_{13}H_{12}NO_2I$). Anal. Calcd: C, 45.75; H, 3.55; N, 4.11. Found: C, 46.30; H, 3.81; N, 3.95.

2-Ethoxycarbonyl-3-(3-iodophenyl)-11-*N*-(*tert*-butoxycarbonyl)-dipyrromethane (3b). To a solution of 2-hydroxymethyl-*N*-(*tert*-butoxycarbonyl)pyrrole[30] (0.90 g, 4.57 mmol) and **2** (1.50 g, 4.40 mmol) in 45 mL of 1,4-dioxane was added aqueous HCl (10%, 9 mL). The reaction mixture was stirred at room temperature for 6 h. Another portion of 2-hydroxymethyl-*N*-(*tert*-butoxycarbonyl)pyrrole (0.30 g, 1.52 mmol) was added, and the reaction mixture was stirred for an additional 12 h. Upon completion of the reaction as judged by TLC (hexanes/ethyl acetate, 4:1), saturated aqueous $NaHCO_3$ (25 mL) and H_2O (50 mL) were carefully added to quench the reaction. The aqueous phase was extracted with ether (4 × 50 mL). The combined ethereal fraction was successively washed with water (3 × 100 mL) and brine (100 mL), dried (Na_2SO_4), filtered, and evaporated. Purification by flash chromatography (silica, hexanes/ethyl acetate, 4:1) separated the two compounds, with regioisomer **3a** eluting first as a colorless solid (0.80 g, 35%) and **3b** eluting second as a colorless solid (1.1 g, 48%). Data for **3a**: mp 55−56 °C; (the ^{1}H NMR and ^{13}C NMR spectra exhibited the effects of rotamers) ^{1}H NMR ($CDCl_3$) δ 1.17 (t, J = 7.2 Hz, 3H), 1.57 (s, 9H), 4.18 (q, J = 7.2 Hz, 2H), 4.58 (s, 2H), 6.10 (m, 1H), 6.24 (t, J = 1.5 Hz, 1H), 6.55 (s, 1H), 7.03 (dt, J = 8.1 Hz, 1.5 Hz, 1H), 7.18 (t, J = 1.5 Hz, 1H), 7.33 (d, J = 8.1 Hz, 1H), 7.56 (d, J = 8.1 Hz, 1H) 7.73 (d, J = 1.5 Hz, 1H), 9.14 (brs, 1H); ^{13}C NMR ($CDCl_3$) δ 14.2, 25.8, 27.9, 59.4, 77.2, 84.3, 93.3, 109.4, 110.6, 114.1, 115.8, 121.4, 125.2, 128.6, 129.1, 131.5, 134.9, 138.2, 138.4, 150.3, 165.3; FAB-MS obsd 520.0880, calcd 520.0859 ($C_{23}H_{25}N_2O_4I$). Anal. Calcd: C, 53.07; H, 4.84; N, 5.38. Found: C, 53.71; H, 4.96; N, 5.43. Data for **3b**: mp 65−66 °C; (the ^{1}H NMR and ^{13}C NMR spectra exhibited the effects of rotamers) ^{1}H NMR ($CDCl_3$) δ 1.14 (t, J = 7.2 Hz, 3H), 1.60 (s, 9H), 4.03 (s, 2H), 4.12 (q, J = 7.2 Hz, 2H), 5.81 (s, 1H), 6.06 (m, 1H), 7.18 (m, 2H), 7.36 (m, 2H), 7.62 (m, 1H), 7.69 (m, 1H), 9.28 (brs, 1H); ^{13}C NMR ($CDCl_3$) δ 14.2, 24.6, 27.9, 59.3, 77.2, 84.3, 93.2, 110.5, 113.3, 114.5, 120.8, 121.2, 122.8, 129.1, 130.1, 132.7, 135.2, 137.4, 139.5, 150.3, 164.7; FAB-MS obsd 520.0878, calcd 520.0859 ($C_{23}H_{25}N_2O_4I$). Anal. Calcd: C, 53.07; H, 4.84; N, 5.38. Found: C, 53.25; H, 4.87; N, 5.20.

3-(3-Iodophenyl)dipyrromethane (4). A 25-mL round-bottom flask was charged with **3b** (1.00 g, 1.92 mmol) and 8 mL of ethylene glycol. The system was flushed with argon for 10 min, and then powdered NaOH (0.20 g, 5.0 mmol) was added and the flask was immersed in an oil bath at 180 °C. The oil bath temperature was increased to 195−200 °C and maintained (total time, 1 h). The reaction flask was then cooled to room temperature and 30 mL of 10% aqueous NaCl was added. The aqueous portion was extracted with CH_2Cl_2 (3 × 25 mL), and the combined organic layers were washed with 50 mL of brine, dried (Na_2SO_4), filtered, and evaporated. Purification by flash chromatography (silica, hexanes/ethyl acetate (3:1) containing 1−2% triethylamine) afforded a gummy solid (0.45 g, 65%): ^{1}H NMR ($CDCl_3$) δ 4.04 (s, 2H), 6.06 (s, 1H), 6.15 (dd, J = 6.0, 3.0 Hz, 1H), 6.30 (t, J = 3.0 Hz, 1H), 6.58 (m, 2H), 7.08 (t, J = 8.1 Hz, 1H), 7.34 (d, J = 8.1 Hz, 1H), 7.54 (dd, J = 8.1 Hz, 1.5 Hz, 1H), 7.67 (brs, 1H), 7.76 (brs, 2H); ^{13}C NMR ($CDCl_3$) δ 25.2, 94.7, 107.1, 108.6, 108.8, 117.0, 117.6, 120.1, 125.6, 126.8, 128.3, 130.2, 134.4, 136.6, 138.8; FAB-MS obsd 348.0144, calcd 348.0124 ($C_{15}H_{13}N_2I$).

Zn(II) 5,10,15-Trimesityl-2-(3-iodophenyl)porphyrin (ZnI β-m). To a solution of 5-mesityldipyrromethane[31] (0.16 g, 0.60 mmol), **4** (0.21 g, 0.60 mmol), and mesitaldehyde (0.18 g, 1.2 mmol) in 100 mL of $CHCl_3$ under argon was added BF_3−etherate (132 μL of a 2.5 M stock solution in $CHCl_3$, 3.3 mM). The reaction mixture was stirred at room temperature for 1 h. DDQ (0.41 g, 1.8 mmol, 3 equiv) was added and stirring was continued for an additional 2 h. The solvent was evaporated under reduced pressure, and the residue was filtered through a silica gel column (hexanes/CH_2Cl_2, 1:1) to remove quinone species and dark pigments. The porphyrin band that eluted first from the column was collected, concentrated to dryness (0.15−0.20 g), dissolved in 50 mL of CH_2Cl_2, and treated with methanolic $Zn(OAc)_2 \cdot 2H_2O$ (0.12 g in 2 mL of methanol). The mixture was heated at reflux for 1 h, then diluted with CH_2Cl_2 (100 mL) and washed successively with saturated aqueous $NaHCO_3$ (2 × 60 mL), H_2O (2 × 60 mL), and brine (60 mL), and then dried (Na_2SO_4), filtered, and concentrated. Chromatography of the crude porphyrin mixture (alumina, hexanes/ethyl acetate, 2:1) afforded the desired porphyrin as the second band (55 mg, 12%): ^{1}H NMR ($CDCl_3$) δ 1.84 (m, 18H), 2.64 (s, 9H), 7.30 (m, 6H), 7.52 (t, J = 8.1 Hz, 1H), 7.97 (d, J = 7.2 Hz, 1H), 8.25 (d, J = 7.5 Hz, 1H), 8.60 (t, J = 2.1 Hz, 1H), 8.73 (s, 4H), 8.87 (m, 2H), 9.30 (m, 1H), 10.15 (s, 1H); LD-MS obsd 931.1; FAB-MS obsd 928.2001, calcd 928.1980 ($C_{53}H_{45}N_4ZnI$); λ_{abs} (toluene) 422, 548, 582 nm; λ_{em} (λ_{exc} = 550 nm, toluene) 587, 642 nm.

5,10,15-Trimesityl-2-(4-iodophenyl)porphyrin (FbI β-m). A sample of ZnI β-m (50 mg, 54 μmol) was dissolved in CH_2Cl_2 (15 mL) and

(30) Tietze, L. F.; Kettschau, G.; Heitman, K. *Synthesis* **1996**, 851−857.

(31) Littler, B. J.; Miller, M. A.; Hung, C.-H.; Wagner, R. W.; O'Shea, D. F.; Boyle, P. D.; Lindsey, J. S. *J. Org. Chem.* **1999**, *64*, 1391−1396.

treated with TFA (30 μL, >5 equiv). The reaction was found to be complete after 1 h as judged by silica TLC, absorption spectroscopy, and fluorescence excitation spectroscopy. Triethylamine (100 μL) was added, and the reaction mixture was stirred for another 10 min. It was then diluted with CH_2Cl_2 (50 mL), washed with 10% aqueous $NaHCO_3$ (2 × 50 mL), H_2O (50 mL), and brine (50 mL), dried over Na_2SO_4, and filtered, and the solvent was removed under vacuum to give a purple solid (35 mg, 78%): ^{1}H NMR ($CDCl_3$) δ −2.72 (brs, 2H), 1.86 (m, 18H), 2.63 (m, 9H), 7.30 (m, 6H), 7.51 (t, J = 7.8 Hz, 1H), 7.98 (d, J = 8.1 Hz, 1H), 8.22 (d, J = 8.1 Hz, 1H), 8.58 (d, J = 1.5 Hz, 1H), 8.64 (m, 4H), 8.77 (s, 1H), 8.81 (d, J = 4.2 Hz, 1H), 9.26 (d, J = 5.1 Hz 1H), 10.10 (s, 1H); LD-MS obsd 868.9; FAB-MS obsd 866.2834, calcd 866.2845 ($C_{53}H_{47}N_4I$); λ_{abs} (toluene) 419, 512, 544, 589, 644 nm; λ_{em} (λ_{exc} = 550 nm, toluene) 646, 715 nm.

Mg(II) 5,10,15-Trimesityl-2-(3-iodophenyl)porphyrin (MgI β-m). A solution of FbI β-m (25 mg, 29 μmol) in 5 mL of CH_2Cl_2 was treated with *N*,*N*-diisopropylethylamine (100 μL, 58 μmol) and MgI_2 (80 mg) with stirring at room temperature. After 30 min, the reaction mixture was diluted with CH_2Cl_2 (30 mL), and then washed with 10% aqueous $NaHCO_3$ (2 × 25 mL), dried (Na_2SO_4), filtered, and concentrated under vacuum to 5 mL. Chromatography (alumina grade V, $CHCl_3$) afforded 22 mg (85%): ^{1}H NMR ($CDCl_3$) δ 1.85 (m, 18H), 2.63 (m, 9H), 7.29 (m, 6H) 7.50 (t, J = 8.1 Hz, 1H), 7.95 (d, J = 8.1 Hz, 1H), 8.27 (d, J = 8.1 Hz, 1H), 8.64 (m, 5H), 8.79 (m, 2H), 9.22 (d, J = 4.2 Hz, 1H), 10.06 (s, 1H); LD-MS obsd 890.8; FAB-MS obsd 888.2556, calcd 888.2539 ($C_{53}H_{45}N_4MgI$); λ_{abs} (toluene) 427, 563, 598 nm; λ_{em} (λ_{exc} = 550 nm, toluene) 605, 660 nm.

Mg(II) 5,10,15-Trimesityl-2-(4-iodophenyl)porphyrin (MgI β-p). Under conditions similar to those described above, a solution of FbI β-p[21] (25 mg, 29 μmol) in 5 mL of CH_2Cl_2 was treated with *N*,*N*-diisopropylethylamine (100 μL, 58 μmol) and MgI_2 (80 mg) to afford 20 mg (78%): ^{1}H NMR ($CDCl_3$) δ 1.83 (m, 18H), 2.62 (m, 9H), 7.29 (m, 6H), 8.09 (AB quartet, J = 6.6 Hz, 4H), 8.62 (s, 4H), 8.75 (d, J = 4.2 Hz, 1H), 8.79 (s, 1H), 9.22 (d, J = 4.2 Hz, 1H), 10.09 (s, 1H); LD-MS obsd 890.0; FAB-MS obsd 888.2557, calcd 888.2539 ($C_{53}H_{45}N_4MgI$); λ_{abs} (toluene) 428, 563, 598 nm; λ_{em} (λ_{exc} = 550 nm, toluene) 604, 659 nm.

Mg(II) 5,10,15-Trimesityl-20-(3-iodophenyl)porphyrin (MgI meso-m). Under conditions similar to those described above, a solution of 5,10,15-trimesityl-20-(3-iodophenyl)porphyrin (FbI meso-m)[3] (31 mg, 36 μmol) in 8 mL of CH_2Cl_2 was treated with *N*,*N*-diisopropylethylamine (120 μL, 0.70 mmol) and MgI_2 (100 mg) to give 25 mg (78%): ^{1}H NMR ($CDCl_3$) δ 1.81, 1.86 (s, 18H), 2.62 (m, 9H), 7.27 (s, 6H), 7.46 (t, J = 7.5 Hz, 1H), 8.07 (d, J = 8.1 Hz, 1H), 8.18 (d, J = 7.5 Hz, 1H), 8.60 (s, 5H), 8.70 (m, 4H); LD-MS obsd 887.9; FAB-MS obsd 888.25, calcd 888.25 ($C_{53}H_{45}IN_4Mg$); λ_{abs} (toluene) 428, 525, 565, 605 nm; λ_{em} (λ_{exc} = 550 nm, toluene) 607, 663 nm.

MgZnU meso-m/p-meso. A solution of FbZnU meso-m/p-meso[3] (12.0 mg, 7.6 μmol) in 5 mL of CH_2Cl_2 was treated with *N*,*N*-diisopropylethylamine (20.0 mg, 0.15 mmol) and MgI_2 (21 mg, 77 μmol) to give 10.0 mg (83%): ^{1}H NMR ($CDCl_3$) δ 1.82 (m, 36H), 2.62 (m, 18H), 7.28 (m, 12H), 7.78 (t, J = 8.1 Hz, 1H), 7.93 (d, J = 8.1 Hz, 2H), 8.06 (d, J = 8.1 Hz, 1H), 8.20 (d, J = 8.1 Hz, 2H), 8.27 (d, J = 7.5 Hz, 1H), 8.57 (s, 1H), 8.63−8.87 (m, 16H); LD-MS obsd 1591.54; FAB-MS obsd 1586.61, calcd 1586.64 ($C_{108}H_{90}MgN_8Zn$); λ_{abs} (toluene) 430, 555, 563, 604 nm; λ_{em} (λ_{exc} = 550 nm, toluene) 608, 664 nm.

MgZnU β-p/p-meso. MgI β-p (20 mg, 23 μmol), Zn(II) 5,10,15-trimesityl-20-(4-ethynylphenyl)porphyrin (ZnU′)[32] (19 mg, 23 μmol), $Pd_2(dba)_3$ (3.2 mg, 3.5 μmol), and P(*o*-tol)$_3$ (8.0 mg, 28 μmol) were added to a 25-mL Schlenk flask. The flask was evacuated and purged with argon three times. Then 9 mL of deaerated toluene/triethylamine (5:1) was added by syringe. The flask was immersed in an oil bath at 37 °C, and the reaction was followed by analytical SEC and found to be complete at 15 h. The solvent was removed, and the crude reaction mixture was dissolved in toluene and loaded on an alumina column (grade V). Elution with toluene/$CHCl_3$ (1:1) afforded the monomeric porphyrin and the desired dimer along with higher molecular weight material as the first band, which was collected and concentrated to dryness. The Pd species remained bound on the top of the column. The porphyrin mixture was dissolved in a minimum amount of toluene, loaded on a preparative SEC column (5 × 65 cm), and eluted by gravity flow with toluene. The desired dimer was obtained as the second band. The dimer solution was concentrated to dryness, dissolved in a minimum of toluene, and chromatographed (alumina grade V, toluene, then toluene/$CHCl_3$, 1:1), affording 20 mg (57%): ^{1}H NMR ($CDCl_3$) δ 1.86 (m, 36H), 2.64 (m, 18H), 7.27 (m, 12H), 8.05 (m, 4H), 8.29 (d, J = 8.1 Hz, 2H), 8.40 (d, J = 8.1 Hz, 2H), 8.65−8.94 (m, 14H), 9.26 (d, J = 4.5 Hz, 1H), 10.20 (s, 1H); LD-MS obsd 1592.79; FAB-MS obsd 1586.61, calcd 1586.64 ($C_{108}H_{90}MgN_8Zn$); λ_{abs} (toluene) 425, 554, 596 nm; λ_{em} (λ_{ex} 550 nm, toluene) 604, 661 nm.

MgZnU β-m/p-meso. Following the same approach as that used for the preparation and purification of MgZnU β-p/p-meso, the reaction of MgI β-m (20 mg, 23 μmol), ZnU′ (19 mg, 23 μmol), $Pd_2(dba)_3$ (3.2 mg, 3.5 μmol), and P(*o*-tol)$_3$ (8.0 mg, 28 μmol) afforded 20 mg (57%): ^{1}H NMR ($CDCl_3$) δ 1.84 (m, 36H), 2.62 (m, 18H), 7.27 (m, 12H), 7.84 (t, J = 7.8 Hz, 1H), 7.92 (d, J = 7.2 Hz, 1H), 8.00 (d, J = 8.1 Hz, 2H), 8.26 (d, J = 7.8 Hz, 2H), 8.37 (d, J = 7.5 Hz, 1H), 8.60 (s, 1H), 8.65−8.90 (m, 14H), 9.28 (d, J = 3.9 Hz, 1H), 10.21 (s, 1H); LD-MS obsd 1592.38; FAB-MS obsd 1586.55, calcd 1586.64 ($C_{108}H_{90}MgN_8Zn$); λ_{abs} (toluene) 425, 553, 592 nm; λ_{em} (λ_{ex} 550 nm, toluene) 602, 659 nm.

MgZnU meso-p/p-meso. Prepared as described in the literature.[13]

MgZnFbU meso-p/p-meso. Prepared as described in the literature.[20]

MgZnFbU meso-m/p-meso. MgI meso-m (10.0 mg, 11.3 μmol), mono-ethynyl ZnFb dimer[20] (17.5 mg, 11.3 μmol), $Pd_2(dba)_3$ (1.6 mg, 1.7 μmol), and P(*o*-tol)$_3$ (4.7 mg, 14 μmol) were added to a 25-mL Schlenk flask. The flask was evacuated and purged with argon three times. After that, 4.5 mL of deaerated toluene/triethylamine (5:1) was added by syringe. The flask was immersed in an oil bath at 37 °C, and the reaction was followed by analytical SEC and found to be complete at 24 h. The solvent was removed, and the crude reaction mixture was dissolved in toluene and loaded on an alumina column (grade V). Elution with toluene/$CHCl_3$ (1:1) afforded the monomeric porphyrin, the dimer, and the desired trimer along with higher molecular weight material as the first band, which was collected and concentrated to dryness. The Pd species remained bound on the top of the column. The porphyrin mixture was dissolved in a minimum amount of THF, loaded on a preparative SEC column (5 × 65 cm), and eluted by gravity flow with THF. The desired trimer was obtained as the second band. The trimer solution was concentrated to dryness, dissolved in a minimum of toluene, and chromatographed (alumina grade V, toluene, then toluene/$CHCl_3$, 1:1), affording 12.0 mg (46%): ^{1}H NMR ($CDCl_3$) δ −2.53 (brs, 2H), 1.85 (m, 48H), 2.64 (s, 24H), 7.29 (s, 16H), 7.79 (t, J = 7.5 Hz, 1H), 7.90 (d, J = 7.2 Hz, 1H), 8.05 (m, 6H), 8.26 (m, 7H), 8.57 (s, 1H), 8.63−8.97 (m, 24H); LD-MS obsd 2306.6; FAB-MS obsd 2306.90, calcd 2306.97 ($C_{160}H_{130}MgN_{12}Zn$); λ_{abs} (toluene) 427, 516, 553, 595, 650 nm; λ_{em} (λ_{ex} 550 nm, toluene) 607, 651, 721 nm.

MgZnFbU β-p/p-meso. Following the same approach as that used for the preparation and purification of MgZnFbU meso-m/p-meso, the reaction of MgI β-p (10.0 mg, 11.3 μmol), mono-ethynyl ZnFb dimer[20] (17.5 mg, 11.3 μmol), $Pd_2(dba)_3$ (1.6 mg, 1.7 μmol), and P(*o*-tol)$_3$ (4.7 mg, 14 μmol) afforded 12 mg (46%): ^{1}H NMR ($CDCl_3$) δ −2.53 (brs, 2H), 1.89 (m, 48H), 2.65 (m, 24H), 7.31 (m, 16H), 8.07 (m, 8H), 8.27−8.42 (m, 8H), 8.65−8.99 (m, 22H), 9.27 (m, 1H), 10.21 (m, 1H); LD-MS obsd 2308.6; FAB-MS obsd 2307.05, calcd 2306.97; ($C_{160}H_{130}MgN_{12}Zn$); λ_{abs} (toluene) 427, 515, 553, 595, 649 nm; λ_{em} (λ_{ex} 550 nm, toluene) 604, 651, 720 nm.

MgZnFbU β-m/p-meso. Following the same approach as that used for the preparation and purification of MgZnFbU meso-m/p-meso, the reaction of MgI β-m (10.0 mg, 11.3 μmol), mono-ethynyl ZnFb dimer[20] (17.5 mg, 11.3 μmol), $Pd_2(dba)_3$ (1.6 mg, 1.7 μmol), and P(*o*-tol)$_3$ (4.7 mg, 14 μmol) afforded 13.0 mg (50%): ^{1}H NMR ($CDCl_3$) δ −2.53 (brs, 2H), 1.87 (m, 48H), 2.65 (m, 24H), 7.30 (m, 16H), 7.85 (t, J = 8.1 Hz, 1H), 7.94 (m, 1H), 8.05 (m, 6H), 8.31 (m, 7H), 8.61 (s, 1H), 8.65−8.98 (m, 22H), 9.30 (d, J = 4.2 Hz, 1H), 10.22 (s, 1H); LD-MS obsd 2310.7; FAB-MS obsd 2306.89, calcd 2306.97 ($C_{160}H_{130}MgN_{12}Zn$); λ_{abs} (toluene) 426, 516, 552, 594, 650 nm; λ_{em} (λ_{ex} 550 nm, toluene) 603, 651, 720 nm.

(32) Lindsey, J. S.; Prathapan, S.; Johnson, T. E.; Wagner, R. W. *Tetrahedron* **1994**, *50*, 8941−8968.

Physical Methods. (a) General. Static and time-resolved absorption and fluorescence studies were performed on samples prepared in toluene at room temperature. Samples for time-resolved fluorescence measurements were degassed by several freeze−pump−thaw cycles on a high-vacuum line; samples for static fluorescence and static and time-resolved absorption measurements were not degassed.

(b) Static Absorption Spectroscopy. Static absorption (Cary 100) measurements were performed as described previously.[8−10,15,28]

(c) Static and Time-Resolved Fluorescence Spectroscopy. Static and time-resolved fluorescence (Spex Fluoromax or Fluorolog II) measurements were performed as described previously.[8−10,15,28]

(d) Time-Resolved Absorption Spectroscopy. Transient absorption data were acquired as discussed elsewhere.[8,9,33] Samples (∼0.1−0.2 mM in toluene or 2-methyltetrahydrofuran) were placed in 2- or 5-mm path length cuvettes at room temperature. They were excited at 10 Hz with 130 fs, 4−6 μJ pump pulses and probed with white light pulses of comparable duration. The kinetic data shown in Figures 2 and 4 were generated by averaging the ΔA values in specific wavelength ranges for the entire set of pump−probe delay times and plotting these values as a function of time. A nonlinear least-squares algorithm was then used to fit the kinetic traces to functions consisting of either a single or a double exponential plus a constant. An Oxford Instruments liquid-nitrogen cryostat was used for low-temperature measurements.

(33) (a) Kirmaier, C.; Holten, D. *Biochemistry* **1991**, *30*, 609−613. (b) Drain, C. M.; Kirmaier, C.; Medforth, C. J.; Nurco, D. J.; Smith, K. M.; Holten, D. *J. Phys. Chem.* **1996**, *100*, 11984−11993.

Acknowledgment. This research was supported by grants from the NSF (CHE-9707995 and CHE-9988142). Mass spectra were obtained at the Mass Spectrometry Laboratory for Biotechnology at North Carolina State University. Partial funding for the Facility was obtained from the North Carolina Biotechnology Center and the NSF.

Supporting Information Available: ^{1}H NMR spectra for all compounds, and LD-MS spectra for all porphyrins and porphyrin arrays (PDF). This material is available free of charge via the Internet at http://pubs.acs.org.

JA001031X